Analysis of the Degree of Reversibility of Crystallization and Melting in Poly(ethylene-*co*-1-octene)

René Androsch[†] and Bernhard Wunderlich*[,‡]

Institute of Material Science, Martin-Luther-University Halle-Wittenberg, Geusaer Str., 06217 Merseburg, Germany, and Department of Chemistry, The University of Tennessee, Knoxville, Tennessee 37996-1600, and Oak Ridge National Laboratory, Chemical and Analytical Sciences Division, Oak Ridge, Tennessee 37831-6197

Received March 21, 2000; Revised Manuscript Received October 5, 2000

ABSTRACT: The degree of reversibility of crystallization and melting of poly(ethylene-*co*-1-octene) containing 7.3 mol % (24 mass %) of 1-octene was measured with temperature-modulated differential scanning calorimetry. The sample was crystallized at different cooling rates after excluding self-nuclei of the crystals. The sample was also examined by X-ray scattering techniques, infrared spectroscopy, and standard differential scanning calorimetry. The cooling rates ranged from 0.1 K min^{-1} to quick quenching. The low-temperature enthalpy remained constant in all cases, by increasingly creating a pseudohexagonal crystallinity of lower heat of fusion instead of a smaller amount of orthorhombic crystals. The crystallization during cooling from the nonseeded melt is characterized by a steplike crystal growth, a characteristic not seen on slow, seeded, crystallization. The initial growth is followed by a continuous increase of the crystallinity down to the glass transition. The onset of crystallization shifts to lower temperatures with increasing cooling rates. With increasing cooling rate, the perfection and the size of the initially formed crystals decrease. On slow crystallization orthorhombic crystals grow; on fast crystallization, these are increasingly replaced by the less-ordered, pseudohexagonal crystals. These changes are paralleled by a systematic increase of the reversible crystallization and melting by about 10% when increasing the cooling rate from 1 to 10 K min^{-1}. For the first time these surprising observations have been discussed on the basis of structural information.

1. Introduction

1.1. Poly(ethylene-*co*-1-octene) and Temperature-Modulated Differential Scanning Calorimetry. The physical structure and the properties of inter- and intramolecularly homogeneous poly(ethylene-*co*-1-octene) are mainly controlled by the constitution of the macromolecule, i.e., the number of hexyl branches in the backbone. The concentration of the branches affects the total crystallinity, the morphology of the crystals, and the crystal structure. As the number of hexyl branches increases, the morphology of the crystals continuously changes from a lamellar structure, typical for standard polyethylene, to a defect-rich, fringed-micellar arrangement.[1] In addition, the orthorhombic crystals are increasingly replaced by monoclinic[2] or pseudohexagonal[3,4] crystals. The crystallinity decreases almost linearly with the comonomer concentration.[1,5−7] The statistical distribution of the hexyl branches in the backbone of the macromolecule can result in a drastically broadened crystallization range, which often covers more than 100 K and can stretch over the entire temperature range from the onset of crystal growth above ambient temperature, down to the glass-transition temperature at 237 K.[8−14]

Previously we found, in accordance with the coexistence of multiple crystal structures, that these copolymers have different crystallization kinetics, as revealed by analyses with temperature-modulated differential scanning calorimetry (TMDSC).[12,13] In the present paper the crystallization and melting behavior of these samples is linked to structural information on the crystals. The TMDSC is a useful tool to separate processes of different kinetics by simultaneous analysis of a sample with an underlying and an oscillating heating rate. The periodic component of the temperature program is typically sinusoidal or sawtooth-like. The underlying heating rate can usually be varied between 0 and 5 K min^{-1} and the oscillating amplitude has been changed in the range from 0.05 to 2 K, and periods between 10 and several hundred seconds have been reported. The resultant modulated heat-flow rate is a superposition of the different thermal responses of the sample to the applied heating rates and can be analyzed by a discrete Fourier transformation. The Fourier analysis permits the separation of the modulated heat-flow rate into a total and a reversing part. The total part is the average over one modulation cycle and approximates the sample response to the underlying heating rate. The reversing part is filtered from the raw data as the amplitude of the first harmonic of the Fourier series and is caused by the response of the sample to the temperature modulation. The nonreversing part, defined as the difference between the total and reversing components, contains therefore all irreversible events that contribute to the higher harmonics of the Fourier series.[15−19] Next, it is customary to calculate the reversing apparent heat capacity, $C_{p,\mathrm{rev}}$, from the amplitudes of the first harmonic of the Fourier series of the heat-flow rate, A_{HF}, and sample temperature, A_{T_s}, according to

$$C_{p,\mathrm{rev}} = \frac{A_{\mathrm{HF}}}{A_{T_s}\omega} K(\omega) \tag{1}$$

where ω is the frequency (2π/period) in rad s^{-1}, and $K(\omega)$ is a calibration function which accommodates the differences between sample and reference calorimeters, as

[†] Martin-Luther-University Halle-Wittenberg.
[‡] The University of Tennessee and Oak Ridge National Laboratory.

10.1021/ma000504h CCC: $19.00
Published on Web 11/10/2000

well as possible changes in temperature gradients within the sample and reference heating paths. In addition to the opportunity to deconvolute thermal events of different kinetics, TMDSC can advantageously be applied to measure relatively slow processes that involve low amounts of latent heat and that often are overlaid by a long-term baseline drift, as in the case of isothermal annealing of polymers.

The reversing component, unfortunately, does not only contain thermal events that reverse completely, like the true heat capacity, but includes also a portion of any event that can be partially reversed within the time and temperature spans of the modulation, and small contributions can also arise from abrupt, irreversible changes that have accidental first harmonic contributions of the frequency ω. Processes that are only partially reversible can be recognized and quantified by analysis of the symmetry of their signal in the time domain, particularly if the experiment is performed quasi-isothermally,[18] i.e., by modulation about a constant temperature T_0 or also by their frequency dependence, if the experiment is performed nonisothermally.[20−22] Note that within the amplitude of temperature modulation a transition may be reversing even if the process is not truly reversible and even if there is no time dependence.[23,24]

1.2. Reversibility of Crystallization and Melting of Polymers. Crystallization and melting of polymers of sufficiently high molar mass are thermodynamically irreversible due to three reasons: (A) The chain-folded crystal morphology causes nonequilibrium crystals. (B) As for most liquids, there is a need for nucleation of a crystal before it can grow. (C) Each macromolecule needs to undergo molecular nucleation before it can add to a crystal. As a result, at a given temperature, crystal and melt do not coexist in dynamic equilibrium.[25−28] Because of this thermodynamic irreversibility, it is expected that polymer crystallization and melting show only a response in the nonreversing part of the modulated heat-flow rate. Exceptions occur when the amplitude of the temperature modulation is sufficiently large to bridge the region of metastability of the polymer melt due to nucleation. Furthermore, TMDSC may exhibit a distortion of the modulation due to recrystallization and annealing processes, governed by the prior thermal history, which can only be removed by using the quasi-isothermal mode of analysis and waiting for a sufficient time to complete the not fully reversible processes. Finally, misrepresentations of the reversing contributions are frequently caused by instrument lags, so that care must be taken in designing the TMDSC experiments for the study of reversing processes.

Reversible changes of the crystallinity with temperature, as will be discussed below for local equilibria and may be possible in multicomponent polymers, must involve low activation energies, so that the overall crystallization and melting rates are sufficiently fast, to maintain equilibrium during the temperature changes of modulation. Primary crystal nucleation can often be avoided by seeding, but molecular nucleation has been suggested to be always necessary as soon as a macromolecule is not attached to a crystal.[25,27] The observation of reversibility of the melt-to-crystal transition is, thus, an indication for the partial attachment to one or more crystals of the macromolecule in question. Molecular nucleation was experimentally discovered by molecular mass segregation of polyethylene during isothermal crystallization from the melt and solution[25,29] and results in a strong molecular mass dependence of the supercooling and the crystallization rates as they were observed, for example, on poly(oxyethylene)s.[30,31] With the establishment of TMDSC, further evidence for molecular nucleation has been collected,[12,13,23,32−35] and a correlation between the crystal morphology and perfection to the degree of reversibility of crystallization and melting has been proposed, based on investigations on samples of different molar mass,[33] molecule architecture,[12,13] and thermal history.[32] In this context, the degree of reversibility is defined as the amount of material that can undergo a truly reversible transition between crystal and melt; i.e., it can be expressed as the change of crystallinity per kelvin.

1.3. Prior Work on the Reversible Melting of Polymers. Truly reversible processes have been quantified for melt-crystallized poly(ethylene terephthalate) in the melting region at 522 K, where the crystallinity changes by about 0.03% per kelvin,[23,32] for poly-ϵ-caprolactone, crystallized isothermally at 328 K with a reversible crystallinity change of about 0.1% per kelvin,[35] for poly(ether ether ketone) at 600 K, with a reversible crystallinity change less than 0.25% per kelvin,[36] and in our earlier work on poly(ethylene-*co*-1-octene) containing between 12 and 25 mass % 1-octene in the entire temperature range between the onset of crystallization during cooling and the glass transition, where the reversible crystallinity change is about 0.1% per kelvin at 299 K for a sample with 24 mass % 1-octene.[12,13] In all this prior work only little structural information was available on the same samples as studied by TMDSC.

It is the scope of this study to modify for the first time the crystal structure and morphology in a defined manner and to explore more quantitatively its influence on the reversibility of the melt−crystal transition. We attempt to quantify the degree of reversibility as a function of the total crystallinity. We assume that the degree of reversibility is related to the number of reversibly attachable and detachable molecule segments on the crystal surfaces.

It may be possible that the earlier identified surface melting of lamellar crystals contributes to this phenomenon (from small-angle X-ray scattering experiments).[37−41] The degree of reversibility, measured in this case on linear polyethylene, is about 0.07% per kelvin at ambient temperature and increases with temperature. The degree of reversibility obtained by TMDSC data by the same authors is similar at ambient temperature and slightly lower at increased temperature (see Figure 10 of ref 41). The authors identified the fold surface as active surface for the reversible crystallization and melting process and classified different polymers according to their ability to undergo sliding diffusion within the crystal. In general, the degree of reversibility of crystallization and melting after fast cooling was found to be increased, compared to slowly crystallized specimens, which is explained by more defects within the crystal, more stretched loops at the fold surface, and by thinner lamella. However, in these studies the reversible event was caused by relatively perfect, lamellar crystals of highly crystalline samples. In the case of the present ethylene−1-octene copolymers with higher 1-octene content, the crystallinity is much lower and lamellar crystals are not the dominant crystal morphology.

Alizadeh et al.[7] considers "secondary crystallization as an efficient, thermoreversible cross-linking phenomenon". The authors did not prove true reversibility; rather, they judged the reversibility of crystallization/melting from nonisothermal measurements of the total crystallinity over a large temperature range, an unacceptable method. It was proposed that secondary and reversible crystallization is due to crystals of small lateral dimensions which may not show a hysteresis between crystallization and melting temperatures. Alizadeh et al. suggest therefore an equilibrium melting and crystallization of entire crystals without any type of nucleation, neither primary surface nucleation nor molecular nucleation.

In the present study we use the cooling rate as parameter to generate different crystal structures and morphologies. The observed differences in the reversibility of crystallization and melting are then discussed on the basis of the changed structure which is characterized by X-ray diffraction and infrared spectroscopy. In general, the phase structure and crystal morphology of copolymers can be controlled by varying the comonomer content or by changing the crystallization conditions. Presently, we prefer to control the crystallization conditions rather than to modify the branch content because of the higher calorimetric precision in the determination of the reversing, apparent heat capacity when the sample within a series of experiments does not need to be removed from the calorimeter and replaced with another one. The nonisothermal crystallization from the melt depends on the chosen cooling rate which affects the final phase and crystal morphology,[12] the onset of crystallization, and the temperature of the melt reached before cooling.[7,42,43] For typical *poly*(ethylene-*co*-1-octene)s an increasing cooling rate shifts the onset of the crystallization to lower temperatures and leads initially to less perfect orthorhombic crystals which are increasingly replaced by pseudohexagonal crystals.

1.4. Prior Work on Poly(ethylene-*co*-1-octene). The ethylene−octene copolymer with 7.3 mol % 1-octene which is used in this study is well-characterized by previous investigations.[3,4,12,13,44] The crystallization, when cooled from the melt at 10 K min^{-1} begins at about 325 K and continues down to the glass transition. The glass transition of polyethylene homopolymer has been established at 237 K with a change in heat capacity of 10.5 J K^{-1} mol^{-1} and does not change much with copolymerization.[45,46] The equilibrium melting temperature of polyethylene is 414.6 K, and the heat of fusion is 4.11 kJ mol^{-1}.[45,47] The total crystallinity of the copolymer calculated with the heat of fusion of the homopolymer is 12−15% at ambient temperature and increases further on cooling, until the glass transition is reached. The copolymers of this type show a distinct tendency for secondary crystallization and annealing. Note that our earlier work[12,13] was misinterpreted by Alizadeh et al.,[7] who claim that we explained the multiple melting behavior exclusively by melting−recrystallization−remelting. In our previous study about irreversible annealing we have quantified time constants for the secondary crystallization process of about 5 min, which must not be considered as melting−recrystallization−remelting and for reorganization of about 100 min at 299 K after cooling with 10 K min^{-1} from the melt, using time-dependent, reversing heat flow measurements in quasi-isothermal TMDSC.[13] We believe that the rigorous statement of completely suppressed classical annealing, i.e., melting−recrystallization−remelting, by Alizadeh et al.[7] is not proven yet by the measurement of the low-temperature annealing peak and final melting temperature at heating rates of 5 and 20 K min^{-1}.

The sample used in our study is at least partially lamellar,[3,4,44] even though a widely accepted classification[1] suggests that its macroconformation is exclusively fringed micellar. Furthermore, we detected a less-ordered pseudohexagonal crystal modification by an additional reflection in the WAXS pattern at about 0.45 nm, with an intensity that is comparable to that of the reflections of the orthorhombic phase. Since we could identify neither higher orders of this reflection nor layer lines, we simply assume a parallel alignment of molecules within crystals of similar lateral size than orthorhombic crystals,[3,4] but which may accommodate more defects, i.e., branches, than the orthorhombic phase. It is likely that the second polymorph is related to the fringed-micellar crystal morphology and exhibits a considerably lower heat of fusion than found for orthorhombic crystals.[3,4]

2. Experimental Section

2.1. Material. The sample used in this study is a commercially available poly(ethylene-*co*-1-octene) from DOW Plastics with 24 mass % (7.3 mol %) (product information by DOW) 1-octene and a molar mass of 78 000 Da. Relevant structural parameters are described elsewhere.[4,12,13] Note that the 1-octene content determined by NMR spectroscopy is 34.5 mass % (11.6 mol %).[5] The samples were given specific thermal histories by changing the temperature of the melt before cooling between 363 and 403 K and by changing the cooling rate from 1 K min^{-1} to that reached by quenching in a dry ice/ethanol mixture.

2.2. Instrumentation. Thermal analyses were performed with a heat-flux differential scanning calorimeter DSC 820 (Mettler-Toledo GmbH) equipped with the ceramic sensor FRS5 and the liquid nitrogen cooling accessory. The furnace was purged with nitrogen at a flow rate of 80 mL min^{-1}. The sample temperature was calibrated using the onset melting temperatures of indium and zinc, extrapolated to zero heating rate, and the preliminary calibration of the heat-flow rate was performed using the heat of fusion of indium. The final calibration of the heat capacity was done with a sapphire as calibration standard. Standard DSC heating scans were performed with 20 K min^{-1} and the cooling scans with 1, 2.5, 5, and 10 K min^{-1} rate of temperature change. Temperature-modulated DSC experiments were carried out quasi-isothermally at 299 K with a sawtooth-modulation controlled at the furnace. The modulated heat-flow rate is separated into a total and reversing component by Fourier transformation, and the reversing heat capacity was calculated using eq 1. The required calibration function $K(\omega)$ was determined as described in detail elsewhere.[48−50] Preferred modulation parameters were a 1.0 K modulation amplitude and a modulation period of 240 s. Additional, complementary TMDSC experiments were performed on the power-compensating DSC 7 (Perkin-Elmer, Inc.) with an intracooler. Temperature calibration was done using the onset melting temperatures of indium and cyclohexane, and the heat-flow-rate calibration was realized using the heat of fusion of indium. The Perkin-Elmer instrument permits a sawtooth modulation which is controlled at the sample temperature sensor.

Wide-angle X-ray scattering (WAXS) experiments were performed with a diffractometer of type URD 63 (Seifert-FPM), operating in the reflection mode using Ni-filtered Cu Kα radiation and a position-sensitive detector (Stoe, FPM). Samples of different thermal history, i.e., crystallized at different cooling rates, were prepared using an evacuated temperature chamber (Paar KG) mounted on the diffractometer. The final calibration of the scattering angle was done with CaF_2 as a standard.

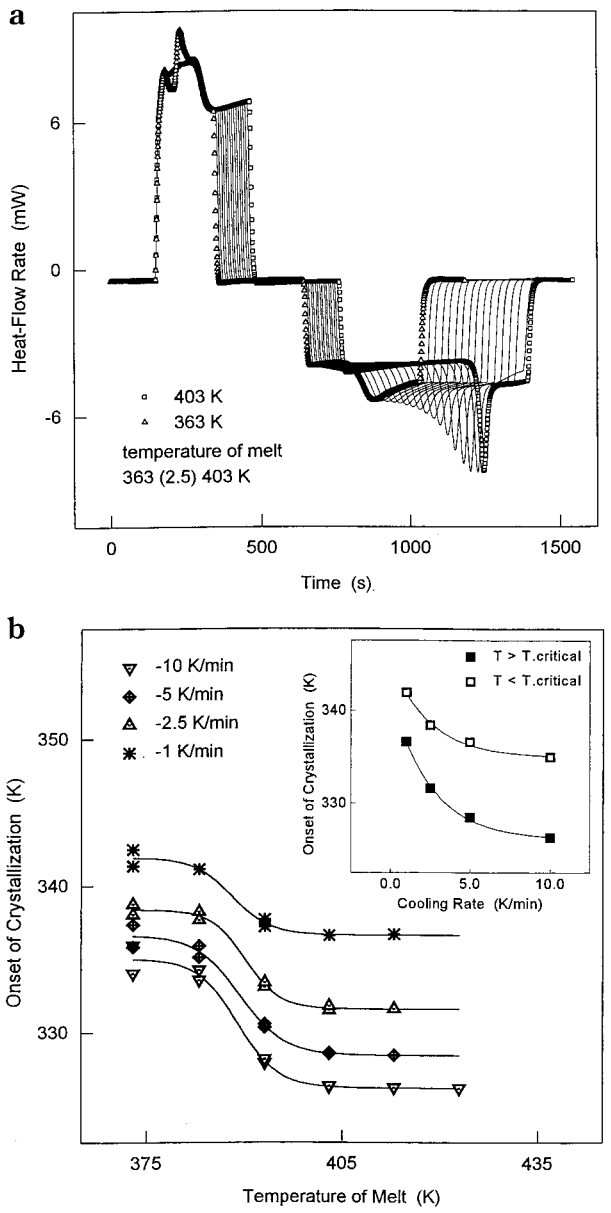

Figure 1. (a) Rate of heat flow as a function of time on heating to different melt temperatures, followed by cooling and crystallization. The sequence of curves refers to the increasing temperature reached by the melt in steps of 2.5 K. All recordings start with isotherms at the left at 298 K and end with isotherms at the right. (b) The onset of crystallization as a function of temperature of the melt and of the cooling rate (inset).

Small-angle X-ray scattering (SAXS) data were recorded with the ORNL area detector at a 5.1 m sample-to-detector distance, using monochromatized Cu Kα radiation and pinhole collimation. The intensity was corrected for background scattering, detector noise, and absorption.

Infrared spectra were taken with the Perkin-Elmer FTIR S2000 system. The samples analyzed had a thickness of 20 μm.

3. Results and Initial Discussion

3.1. Self-Nuleation. Figure 1a displays a series of standard DSC heating and cooling traces in the time domain. The data show the influence of the temperature of the melt on the crystallization during subsequent cooling. The sample was heated always with 20 K min^{-1} from 298 K to different temperatures in the melt, kept there for 5 min at the maximum temperature, and then cooled with 10 K min^{-1} back to 298 K. The maximum temperature of the melt was varied systematically from 363 to 403 K in steps of 2.5 K. The first heating scan shows a distinct annealing peak before final melting; all subsequent heating traces feature only minor changes in their melting behavior as a function of the maximum temperature of the melt reached before crystallization. The crystallization, however, strongly depends on the temperature of the melt reached before cooling, as can be seen by the altered shape of the crystallization exotherm and the peak temperatures of the crystallization on the right side of Figure 1a.

In Figure 1b the onset of the crystallization is plotted for a series of different cooling rates (see also the insert) versus the temperature of the melt before cooling. The melting process is completed at about 355−360 K. The onset of crystallization decreases by about 8−10 K for the case of cooling at 10 K min^{-1} when the temperature of the melt increases from ca. 380 to 400 K. This decrease of the crystallization temperature also depends on the applied cooling rate. At a cooling rate of 1 K min^{-1} the difference is only about 4 K (see the inset in Figure 1b).

The change of the crystallization temperature as a function of melt temperature can be explained by crystal nucleation phenomena.[25,51,52] As long as the temperature of the melt is lower than a critical value, e.g., 380 K, primary nuclei are not destroyed under the chosen conditions, and crystallization on cooling occurs at a higher temperature since the activation energy for initiation of crystallization is lowered by self-nucleation.[51] By extending the time of holding of the melt at the maximum temperature no changes were observed. The types of the remaining nuclei were not explored; however, the conditions were found to completely destroy the thermal history prior to the crystallization experiment.

We also need to point out that, in our previous study of the annealing behavior on a series of different poly(ethylene-*co*-1-octene), one of the samples differed in its crystallization behavior (ref 13, Figure 1a, sample 3). We know now that all of these samples with a comonomer contents between 12 and 25 mass % show the same crystallization behavior as the sample featured in this research when they exceed critical melt temperatures of 380−400 K. The independence of the critical temperature on the comonomer concentration points to a complete exclusion of the branches from a particular crystal fraction which may remain as homogeneous nuclei up to a temperature of about 400 K, close to the equilibrium point of polyethylene. We use the data of Figure 1a,b to establish reproducible conditions for crystallization without self-nucleation. Except when stated otherwise, the further experiments, to be described below, were carried out with samples that were heated to 403 K prior to the crystallization.

3.2. Crystallinity. Figure 2 shows the apparent specific heat capacity, calculated from the standard DSC cooling and heating traces. The samples were crystallized on cooling at rates of 2.5, 5, and 10 K min^{-1}and then melted on heating at 20 K min^{-1}. The apparent specific heat capacities during cooling are recorded as negative, to separate them from the heating traces. Additionally, data from the first heating scan are shown by the dashed line.

On cooling with an increasing rate, the onset of crystallization shifts to lower temperatures, and the

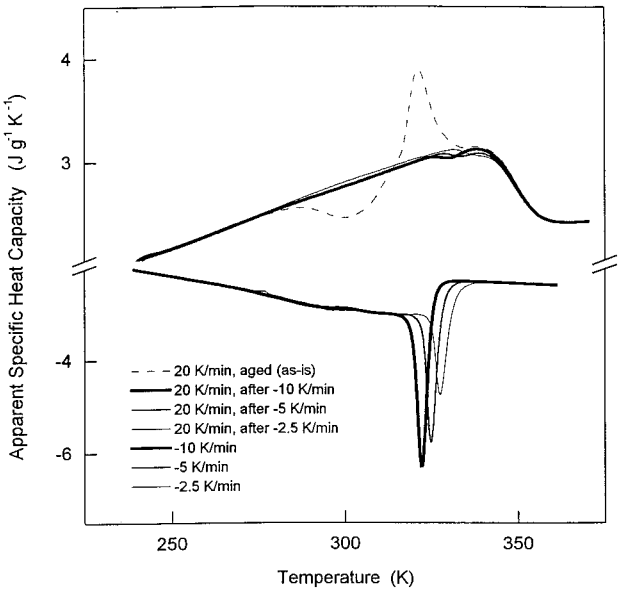

Figure 2. Apparent specific heat capacity as a function of temperature, calculated from standard DSC experiments. The data obtained from cooling scans are multiplied with (−1) for clarity. The sample was heated to 403 K before cooling. The dashed line indicates the initial heating experiment. The rates of temperature change are listed in the figure.

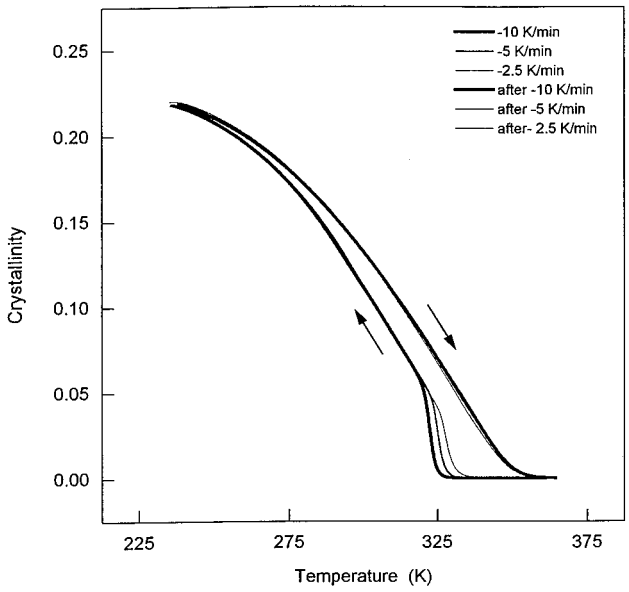

Figure 3. Crystallinity, expressed as mass fraction, as a function of temperature, calculated using the data of Figure 2 and the heat of fusion of orthorhombic polyethylene.

initial crystallization peak increases. After the initial crystallization is completed, the apparent specific heat capacity is the same for all cooling rates. The heating scans, in turn, are only slightly affected at the temperature close to final melting. The first run of the sample is marked by the dashed line. It shows the a minimum followed by a maximum, a typical annealing peak, indicating recrystallization and reorganization that occurred with this sample before its initial use.[13]

The enthalpy-based crystallinity, as derived from the apparent heat capacity measured on cooling and the heat of fusion of the orthorhombic polyethylene, is shown in Figure 3. The sharp crystallization exotherm is clearly mirrored in the initial, steplike increase in crystallinity before the more gradual increase that

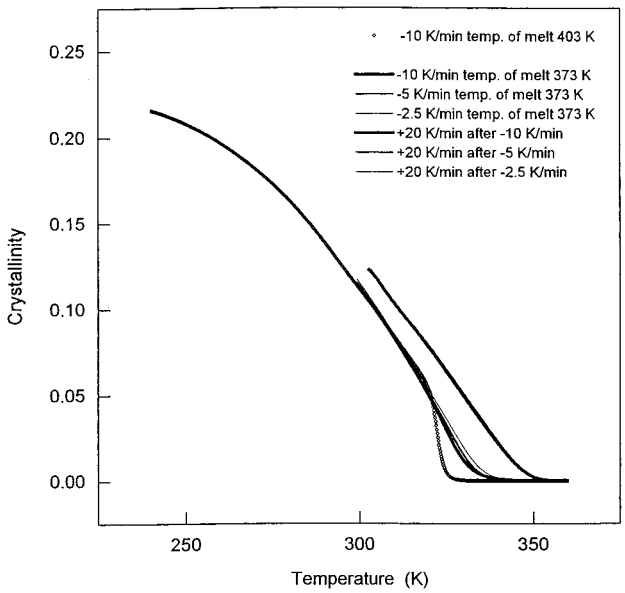

Figure 4. Crystallinity as a function of temperature as in Figure 3, but the sample was heated to only 373 K before cooling, instead of 403 K. (Curve marked with ◇ was cooled from 403 K, for comparison.)

continues up to the glass transition temperature of about 237 K.[13] The initial step of the crystallinity is larger if the sample is cooled at a higher rate. At a cooling rate of 10 K min^{-1}, the crystallinity increases from 0 to 5%, and at a cooling rate of 2.5 K min^{-1}, the crystallinity increases from 0 to about 3%. Although the absolute changes in crystallinity are small, the relative changes are not and reach as much as 60%. Despite these differences of the initial crystallinity, all curves merge, and the final crystallinity based on the heat of fusion of orthorhombic polyethylene is close to equal for all cooling rates.

The decrease of the crystallinity on heating, also shown in Figure 3, is almost independent of the previous cooling rate and does not lead to a steplike decrease that would parallel the cooling. Figure 3 can barely resolve differences in the heating scans. It is not possible to extract from the standard DSC data of Figures 1−3 any information about possible reversing, or even reversible processes, as was recently done by Alizadeh et al.[7] Note that it is customary in TMDSC to call all contributions to the first harmonic of the heat-flow response to the temperature modulation *reversing*, while the label *reversible* requires proof of global or local thermodynamic reversibility, i.e., the absence of supercooling, superheating, and instrumental or computational artifacts.

In Figure 4, the same types of crystallinity data are reproduced for samples that did not exceed the critical temperature of the melt before cooling. The temperature of the melt before cooling was 373 K, in contrast to 403 K, used for the experiments shown in Figure 3 (compare to the curve marked with ◇). The crystallization begins at considerably higher temperature, and more importantly, the kinetics of the initial crystallization is completely changed. The typical steplike increase of the onset of crystallization in Figure 3 is replaced in Figure 4 by a more gradual increase (disappearance of the crystallization peak). Except for the loss of the initial crystallization peak, there are no other major changes in the crystallization and melting behavior.

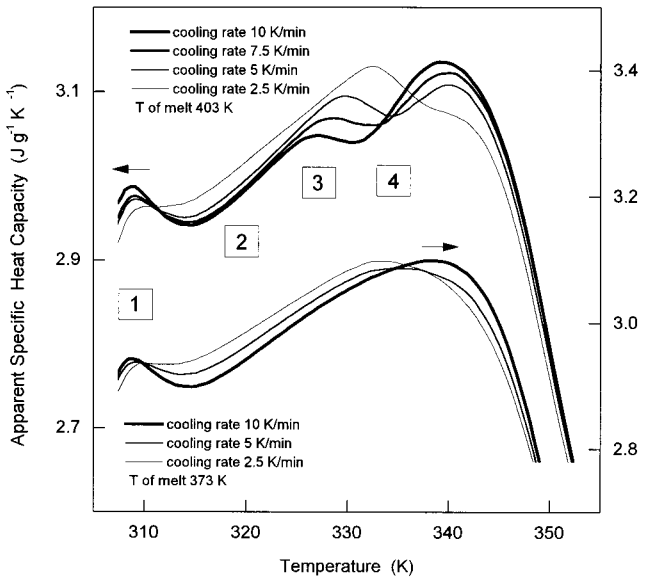

Figure 5. Apparent specific heat capacity as a function of temperature in the melting range, calculated from standard DSC experiments, run after holding for 10 min at 298 K. The samples were heated to 403 K before cooling (upper curves) or to 373 K (lower curves).

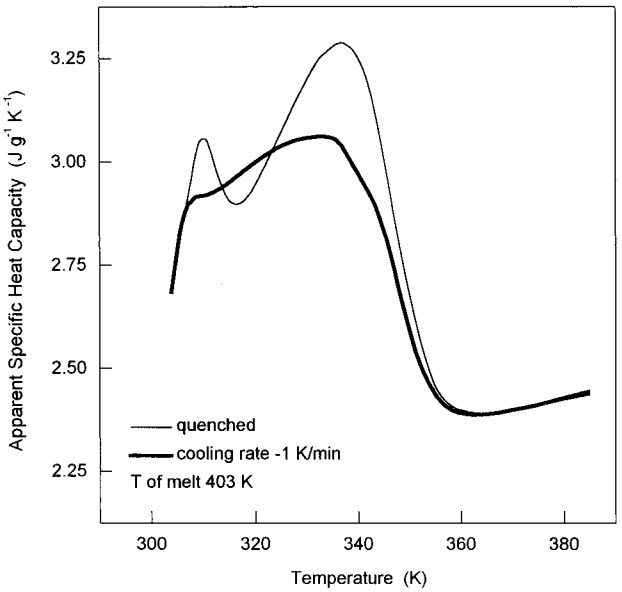

Figure 6. Apparent specific heat capacity on heating as a function of temperature in the melting range, calculated from standard DSC experiments, run after holding for 10 min at 298 K. The samples were heated to 403 K before fast quenching (thin line) or cooling with the slow rate of 1 K min^{-1} (heavy line).

A magnification of the differences in the melting effects that can hardly be discerned in Figure 2 is given in Figure 5. The samples were reheated with 20 K min^{-1} after cooling at different rates from 403 K (upper curves) or 373 K (lower curves). In contrast to the samples in Figures 1−4, the samples of Figure 5 were held for 10 min at 298 K for some annealing before heating. The first maximum [1] of the apparent specific heat capacity occurs in both sets of curves. It is the annealing peak due to the isothermal holding at 298 K before heating. It becomes smaller with a decreasing rate of prior cooling, as is expected for the better crystals that result from the slower cooling.[25] The second systematic change [2] is also caused by the variation of the cooling rate. The level of the apparent specific heat capacity reached in the temperature interval following the annealing peak [1] is lower for faster cooling in both sets of data. The absolute level of the self-seeded samples in the bottom curves, however, is lower than that of the samples not self-seeded, so that the 2.5 K min^{-1} trace of the lower set of curves approximately matches the 10 K min^{-1} data of the upper curves.

Next, the final melting starts with a decrease in apparent specific heat capacity in area [3], followed within a very few degrees with the onset of the melting peak at [4]. This again appears like an annealing peak, superimposed on the broad maximum in the apparent specific heat capacity. This annealing peak seems to be directly related to the initial, steplike increase of the crystallinity during cooling, seen in Figure 3. It does not exist in the self-seeded samples of the lower curves in Figure 5. A higher cooling rate results in a larger crystallization exotherm, lower crystallization temperature, and thus also poorer crystals. Consequently, the annealing peak developed on heating starts at lower temperature for the faster prior cooling rates, and the corresponding annealing peak increases in size. The self-seeded samples show also some signs of annealing on heating. The faster cooled samples melt at higher temperature due to a larger amount of perfection during the heating.[25,26]

The higher apparent specific heat capacity at [2] before final melting of samples cooled more slowly may be caused by the longer time available for secondary crystallization during slow cooling, which results in a slightly higher crystallinity and perfection of low-melting material and consequently a lower annealing peak [1]. The difference of the crystallinity can be estimated from the apparent heat capacity differences. A difference in specific heat capacity of 0.04 J g^{-1} K^{-1}, as seen in Figure 5, would lead over a temperature range of 20 K to a latent heat of 0.8 J g^{-1} or a crystallinity of about 0.25% (orthorhombic equivalent). The lower level of the apparent specific heat capacity of the self-seeded samples is probably due to the difference between the initial orthorhombic and pseudo-hexagonal crystallinities to be discussed below.

These differences in type and level of crystallinity caused by seeding and cooling rate hardly can be important for practical purposes, but the change in overall morphology they induce may be. The data shown in Figure 5 were gathered under most reproducible conditions by keeping the same sample in the calorimeter and realizing cooling rates that permit quantitative analysis free of undue lags. With Figure 6 the limits of this type of experiment were explored. Cooling was speeded up by quenching outside of the calorimeter in a dry ice/ethanol mixture. The standard heating scan following such faster cooling is then compared to a measurement as done for Figure 5 but cooled at the slow rate of 1 K min^{-1}, which also reduces the precision of the heat capacity. These limiting data show the same features as outlined in the discussion of Figure 5 but are even more distinct. Striking is that the sample quenched in dry ice/methanol shows an overlap of the two annealing peaks and a region [2]. The very slowly cooled sample shows practically no annealing peaks.

3.3. X-ray Structure. Figure 7 shows WAXS diffractometer scans from the samples that were cooled with 1, 5, 10, and 20 K min^{-1} or quenched in a dry ice/ethanol mixture. The patterns were taken immediately after

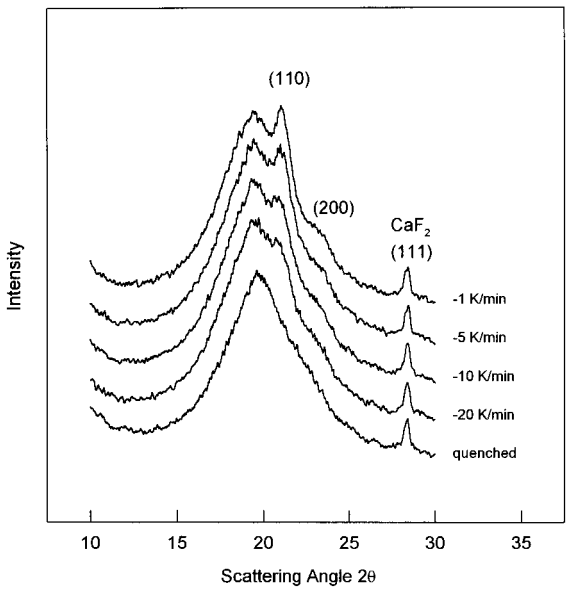

Figure 7. WAXS diffractometer scans (intensity versus scattering angle 2θ) on isotropic samples, cooled at different rates.

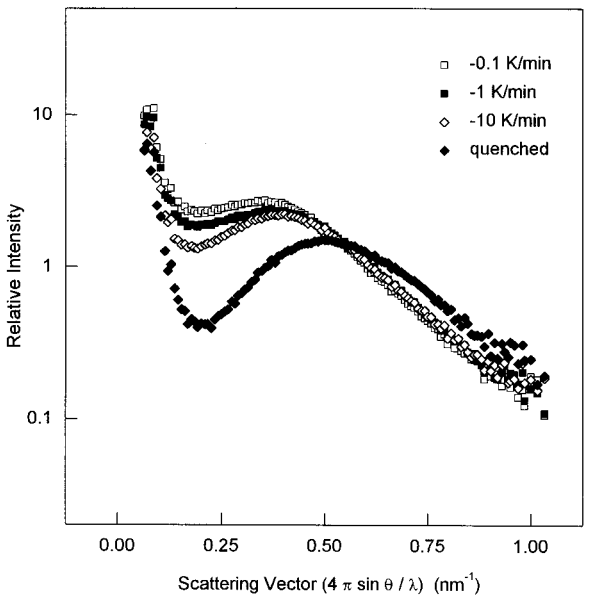

Figure 8. SAXS intensity as a function of the scattering vector for isotropic samples, cooled at different rates.

Table 1. SAXS Long Period *L* of Poly(ethylene-*co*-1-octene) (7.3 mol % 1-Octene), Cooled at Different Rates

cooling rate (K min^{-1})	*L* (uncorrected) (Å)	*L* (Lorentz-corrected) (Å)
−0.1	179	132
−1	166	126
−10	159	123
quenched	125	103

cooling, although we had proven in an earlier study that during annealing no changes occur in the WAXS pattern.[12] In the present work, we repeated these measurements to establish a direct correlation of the structure measured by WAXS to the degree of reversibility of crystallization, crystallinity, and melting and crystallization characteristics, as measured by calorimetry. The sample cooled at 1 K min^{-1} clearly exhibits the 110 and 200 reflections from some orthorhombic crystals. The peak at 28.28° (2θ) is the 111 reflection of CaF_2, included for calibration of the scattering angle. With increasing cooling rates, the intensity of the 110 and 200 reflections from the orthorhombic crystal structure decrease, and in the case of the quenched sample, these reflections completely disappear. We have, however, no information that the orthorhombic structure has, indeed, completely vanished. Because of crystal size and disordering effects, the characteristic 110 and 200 reflections may be broadened such that they cannot be identified anymore. The remaining diffraction, however, is not only the amorphous halo, but there is an additional reflection, originating from a pseudohexagonal phase, identified earlier and discussed in sections 1.1 and 1.4.[3,4] The crystallinity observed by standard DSC is unchanged and independent of the cooling rate, as documented in Figures 3 and 4. We simply assume that with increasing cooling rate the hexyl branches, which can only be incorporated to a limited amount into the orthorhombic crystal structure,[53,54] create at higher supercooling a less-ordered structure that averages to a cylindrically symmetric motif and seems to affect a larger fraction of the polymer.

Naturally, the question of the physical meaning of the term "crystallinity" arises when determining it from latent heats measured by DSC on the basis of the heat of fusion of orthorhombic polyethylene when there is no quantitatively matching X-ray crystallinity. The heat of fusion of a less-ordered, macroscopically more symmetric polyethylene crystal, which is in an overall metastable state, should be less than that of the perfect orthorhombic crystal. The heat of fusion of the pseudohexagonal crystal structure has been estimated for various samples ranging from the fully crystalline mesophase at high pressure[55] to the oriented amorphous phase in gel-spun ultrahigh molar mass polyethylene fibers.[56] Values between $^1/_3$ and $^1/_2$ of the heat of fusion of the orthorhombic structure seem most reasonable. Therefore, it must be concluded that the DSC crystallinity based on the heat of fusion of the orthorhombic crystals can serve only as a benchmark for comparison, but it most likely underestimates the actual phase content by, perhaps, 50% or even more. The X-ray crystallinity of other samples of poly(ethylene-*co*-1-octene) was found to be 25%, while the crystallinity by DSC was only 12−15%.[3,4]

In Figure 8, SAXS patterns are shown which were obtained on isotropic samples after azimuthal integration of the circularly symmetric, two-dimensional scattering. After cooling from 403 K at different rates, the samples were stored before the measurement at ambient temperature until structural equilibrium was reached.[13] Table 1 contains a summary of the calculated long period, *L*, using Bragg's law, from both the uncorrected and the Lorentz-corrected data. Since no information about the lateral dimension of the assumed lamellae is available, we cannot favor either of the two data sets.[57] Therefore, the listed long periods in Table 1 must be considered as upper and lower limits. The relative changes, however, are almost independent of the correction. As the cooling rate is increased by 1 order of magnitude, we can see a systematic decrease of the long period by about 3−5%. In the case of the quenched sample, the decrease is somewhat larger and the peak is much broader; however, the exact cooling rate is unknown.

The independence of the enthalpic crystallinity on cooling rate at ambient temperature (Figure 3) goes

along with the approximate constancy of the SAXS invariant [$Q = \Omega(1 - \Omega)(\rho_1 - \rho_2)^2$, with Ω and ρ representing the volume crystallinity and the electron density of the different phases]. The WAXS data shown in Figure 7 and the FTIR data, which we discuss in the next section, strongly suggest an overall decrease of the perfection/density of the crystalline phase. Therefore, the constancy of the enthalpic crystallinity, as well as of Q, must be explained by a larger volume fraction of the crystalline phase with a decreased density. The decrease of the small-angle Bragg distance with an increasing cooling rate, therefore, must be due to a higher number of smaller crystals; i.e., we have a very reasonable proof of an average increase of the surface-to-volume-ratio of the crystalline phase. Additional information may be available if we would consider that the increased number of lattice defects in form of kinks, as the result of an increased gauche-bond concentration, shortens the crystal in the chain direction up to 10% if the number of involved repeating units is maintained.[58] It should be noted that the decrease of the melting temperature with increasing cooling rate, the event marked [3] in Figure 5, is in good accord with the just described observations.

3.4. FTIR Results. Figure 9a displays the FTIR spectra of the poly(ethylene-*co*-1-octene) cooled at different rates from the melt at 403 K to ambient temperature in the wavenumber range from 675 to 775 cm^{-1}, which shows the CH_2 rocking band at $\nu = 721$ cm^{-1}. In the presence of the orthorhombic crystal structure, this absorption splits into two components at 721 and 730 cm^{-1} due to the 2-fold symmetry axis within the crystal. Since the absorption at 730 cm^{-1} is only observed in the presence of orthorhombic crystals, the doublet can give information about the crystallinity and degree of orientation.[59] The spectra of Figure 9a clearly show the absorption at 730 cm^{-1}, which weakens with increasing cooling rate, and in the case of the quenched sample, the crystalline band has almost completely disappeared. These spectra parallel the WAXS results. The absorbance of the quenched sample of the somewhat broadened 721 cm^{-1} band, however, suggests still a separable shoulder at the higher wavenumber side.

More information can be gained by the calculation of the second derivative of the spectra as shown in Figure 9b. Forming of the second derivative is used as a mathematical tool for the separation of strongly overlapping signals.[60] The second derivative resolves an additional signal at approximately 716 cm^{-1} which is due to a second crystal polymorph. With increasing cooling rate the intensity of the 720 and 730 cm^{-1} absorbance is decreased, and that at 716 cm^{-1} is increased. The data clearly suggest that the decrease of the intensity of the 110 and 200 reflections in the WAXS pattern is not only due to an increased imperfection and/or decreased size of the orthorhombic crystals but also due to a decreased amount of orthorhombic crystals, at the expense of a second, less ordered polymorph. The absorbance at 716 cm^{-1} is often interpreted by the existence of the monoclinic crystal form, mainly observed in deformed specimens[61,62] but, more important, was also obtained in quenched specimens of polyethylene single crystals.[63] We cannot argue whether the second polymorph is indeed a three-dimensional monoclinic phase or a disordered, pseudohexagonal mesophase. It is a matter of fact that neither our X-ray study[3,4] nor the complementary X-ray investigation of

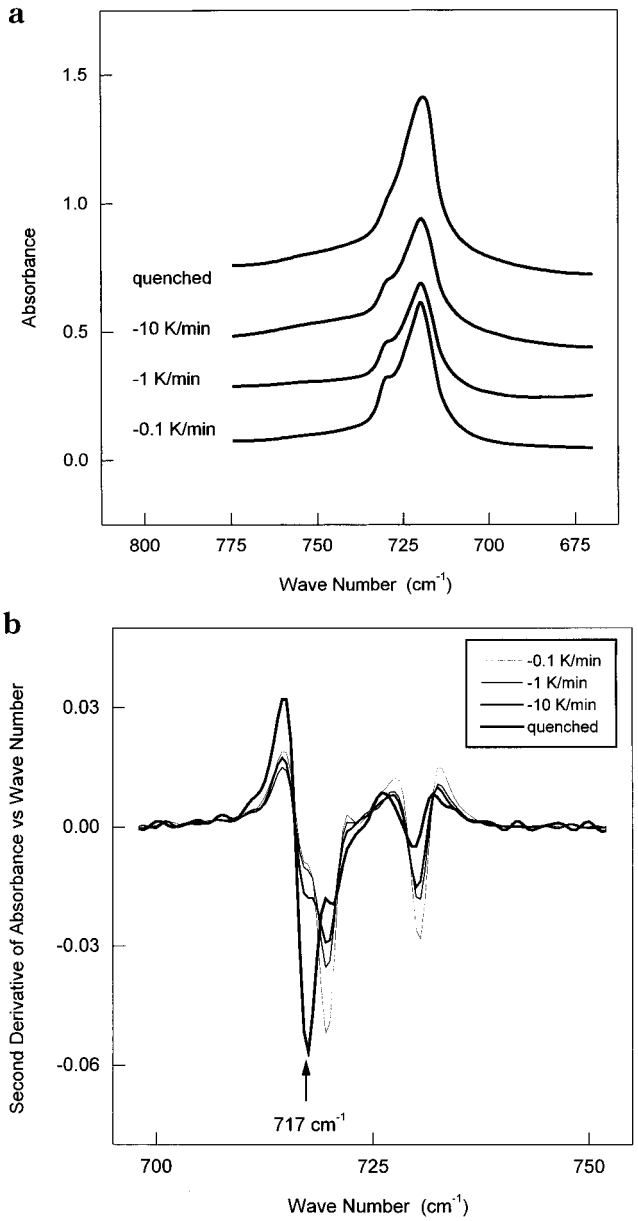

Figure 9. (a) FTIR spectra (absorbance versus wavenumber) of samples cooled at different rates from 403 K to ambient temperature, in the frequency region of CH_2 rocking. (b) Second derivative of the FTIR spectra of (a).

the above-mentioned infrared study on quenched and annealed polyethylene single crystals[63] could verify a truly three-dimensional monoclinic crystal polymorph.

3.5. Reversible Melting and Crystallization. Figure 10 shows the reversing, apparent specific heat capacity as a function of time. The three curves were measured quasi-isothermally at 299 K after cooling from the melt at 403 K with rates of 2.5, 5, and 10 K min^{-1}. The reversing specific heat capacities decreases with time due to recrystallization and reorganization, as was discussed earlier.[13] With decreasing cooling rate, the level of the apparent reversing heat capacity is shifted to lower values. Extending the annealing until a steady state is reached; i.e., until the apparent specific heat capacity becomes truly reversible, the difference between the samples is maintained. The data are generated with a sawtooth-like modulation and are measured at a frequency of $2\pi/120 = 0.0524$ rad s^{-1} (0.008 33 Hz) but are not frequency-corrected (as has been worked out

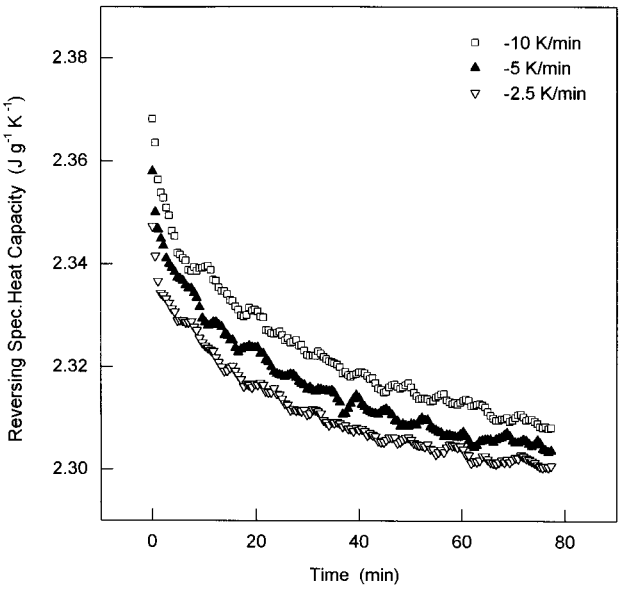

Figure 10. Reversing, apparent specific heat capacity after cooling from 403 K at 2.5, 5, and 10 K min^{-1}, measured quasi-isothermally at 299 K (modulation period 120 s, modulation amplitude of 1.0 K).

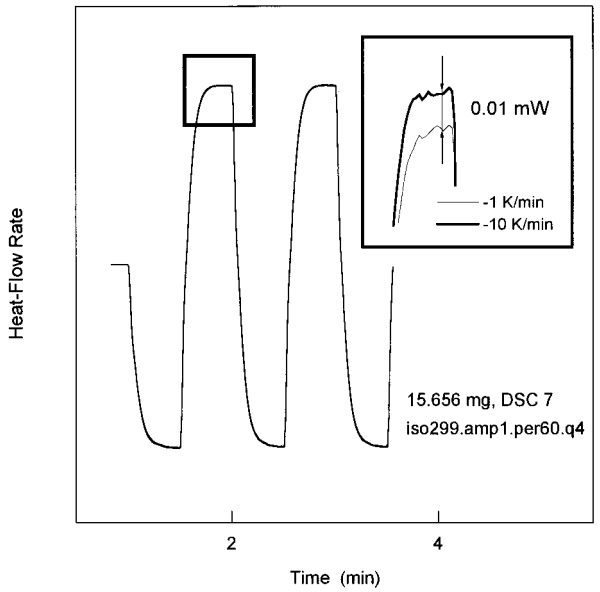

Figure 11. Modulated heat-flow rate as a function of time, measured quasi-isothermally at 299 K (modulation period 60 s, modulation amplitude 1.0 K) after cooling from 403 K at 1.0 and 10 K min^{-1} and annealing for 900 min, using the Perkin-Elmer DSC 7.

for the different calorimeters[48−50]). The corrected values would lead to an even higher reversing apparent specific heat capacity.

It is the scope of this study to explore the cooling-rate dependence, and therefore the structure dependence, of the steady-state, reversing heat capacity, i.e., the truly reversible latent heat component in the heat capacity. In a previous study performed with the same material we found a corrected, completely reversible, excess apparent specific heat capacity of 0.28 J g^{-1} K^{-1} (at 299 K, after cooling with a rate of 10 K min^{-1}). In the present experiments we need to discuss differences in heat capacity of the order of 0.01 J g^{-1} K^{-1} for the samples cooled at different rates to support the observation that a local equilibrium in the overall metastable structure is the cause of this reversible crystallization and melting and that it can be affected not only by changes in the copolymer composition[13] but also by the morphology. For the discussion of the (uncorrected) reversible specific heat capacities shown in Figure 10, we require an accuracy in the heat capacity determination of better than about 0.4%. This approaches the limit of precision of scanning calorimetry. These small, systematic, and reproducible differences in the apparent specific heat capacities need, thus, to be verified by several parallel experiments, to be summarized next.

We have measured the reversing apparent specific heat capacity (1) by using different calorimeters (the heat-flux DSC 820 by Mettler-Toledo and the power-compensating DSC 7 by Perkin-Elmer), (2) by analyzing samples that were externally crystallized in the WAXS temperature chamber (crystallized, followed by annealing at ambient temperature for several days), and (3) by comparing TMDSC and standard DSC data. Figure 11 shows two typical raw heat-flow curves measured on samples that were cooled with 1.0 and 10 K min^{-1} and annealed for 900 min at 299 K using the Perkin-Elmer DSC 7 (60 s period, 1.0 K amplitude, and modulated rate of temperature change of ±4 K min^{-1}). The inset shows an enlarged portion of the otherwise not visible difference in the heat-flow amplitude, which is about 0.01 mW, and with a sample mass of 15.66 mg the

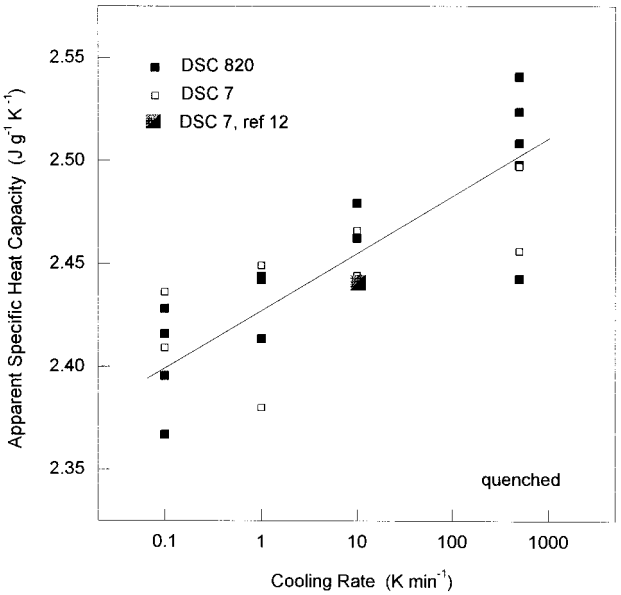

Figure 12. Apparent specific heat capacity of annealed samples at 299 K as a function of the cooling rate. For comparison, the liquid specific heat capacity is 2.20 J K^{-1} g^{-1}, and that of the orthorhombic crystals is 1.55 J K^{-1} g^{-1}.

reversing specific heat capacity is about 0.01 J g^{-1} K^{-1}, the same magnitude as shown in Figure 10. Next, in Figure 12 specific heat capacity data are summarized for samples that were crystallized outside the calorimeter and measured with the two different instruments. The data unambiguously verify the observations of Figures 10 and 11. The reversing, apparent specific heat capacities decrease with a decreasing cooling rate. A further proof is given in Figure 13 with cooling scans of standard DSC, performed after annealing of differently cooled samples at 299 K. Steady state is approached after about 120 min in the lower set of curves, but not in the upper ones. One expects such annealing to have produced a metastable sample that does not rearrange further for a small amount of additional cooling. Indeed,

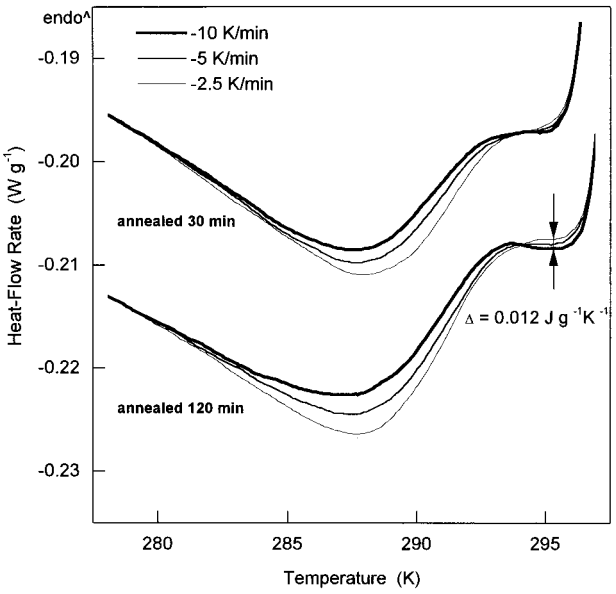

Figure 13. Standard DSC cooling scans of differently cooled samples after annealing for 30 and 120 min at 299 K.

as soon as the calorimeter reaches its steady-state heat-flow rates (at about 296 K), an almost constant heat flow is measured which corresponds to the local equilibrium reached after the annealing at 299 K (compare the plateaus marked by the double arrows). The level of the heat-flow rate is, again, determined by the prior cooling rate. Below 294 K, the heat-flow rates of the different samples cross, due to renewed changes in the metastable structural equilibrium on further cooling (see ref 13, Figure 3). The differences of the heat-flow rate in the limited temperature range of equilibrium is about 0.01 J g^{-1} K^{-1}, as also seen in Figure 12. The interpretation of this change in reversible heat capacity with morphology is discussed in the next section.

4. Conclusion and Final Discussion

4.1. Summary of the Thermal Behavior and Structure Analysis. The temperature range of crystallization and melting of the here analyzed poly(ethylene-*co*-1-octene) lies between the glass and initial crystallization or final melting temperatures. Such broad range of transition for polyethylene was first documented some 35 years ago.[14] Although the crystallization behavior varies strongly when changing the nucleation mechanism (see parts a and b of Figure 1) and the cooling rate (see Figure 2), the ultimate decrease in enthalpy relative to the liquid polymer is close to the same for all conditions and can be expressed in terms of a hypothetical orthorhombic crystallinity (see Figures 3 and 4). Assuming a lower heat of isotropization for the pseudohexagonal mesophase, as suggested in section 3.3, increases the crystallinity at the glass-transition temperature to as much as 50%. The annealing and melting behavior, which is linked to the difference in crystal structure and morphology, can be extracted from standard DSC traces. Summarizing the discussion of the standard DSC heating scans in Figures 5 and 6 permits a discussion of the thermal history; i.e., the heating scans can be used as a fingerprint which characterizes the thermal history of the material when taking into account the well-known annealing behavior during heating studied for many polymers:[26]

(1) Overall, more slowly cooled crystals have more perfection when being grown at the same temperature with or without self-nucleation. The higher apparent heat capacity seen over the temperature range from the glass transition to perhaps 340 K signifies a higher amount of melting of small crystals (see Figure 5). The total crystallinity involved over this 100 K range is no more than 1.0% crystallinity when calculated with the orthorhombic heat of fusion (see section 3.2).

(2) This basic premise of better crystals on slower cooling is supported by the annealing peaks, one at low temperature, induced by annealing at 298 K, the other at high temperature, caused by heating through the temperature range of quick crystallization in the peak area seen in Figures 1 and 2. Annealing at 298 K results in annealing peaks in both seeded and not seeded crystals. As was shown before, the annealing temperature almost exactly corresponds to the temperature position of the apparent heat capacity minimum.[13] Since discrete crystallization peaks are found only in not self-seeded crystals, there are no second annealing peaks in the self-seeded samples (see Figure 5, bottom curves).

(3) The magnitudes of all annealing peaks or shoulders are proportional to the cooling rates; i.e., their sizes are proportional to crystal imperfection. The crystals grown in the initial, sharp crystallization peak seen in Figure 2 are poorer when grown faster and at lower temperature; i.e., on heating they lead to more crystal perfection and the observed larger annealing peaks.

(4) The continuous high-temperature annealing noticeable for the seeded crystals is similarly proportional to the prior cooling rate and signifies that faster crystallization yields poorer crystals. The slightly lower level of the apparent heat capacity of the seeded crystals indicates that the overall crystallinity in the temperature range above 320 K is higher (the seeded sample cooled at 2.5 K min^{-1} corresponds approximately to the not seeded sample cooled at 10 K min^{-1}). The almost constant overall lowering of enthalpy on crystallization is thus due to a compensation of larger and smaller crystals.

The component of the crystallinity that can be identified by WAXS and FTIR as the common orthorhombic crystal decreases toward zero when crystallizing at lower temperature, leaving mainly the pseudohexagonal, mesophase component (see Figures 7 and 9). This loss of orthorhombic crystals is gradual, and no "transition" from one mode of crystallization to the other can be identified. The average size of the crystals at ambient temperature, judged by X-ray analysis and the melting temperature (see Figure 5, the event marked with [3]), decreases with an increasing cooling rate. Both smaller crystals and an increased number of less-dense crystals contribute to the decrease of the small-angle Bragg distance.

Finally, there is a certain reversible contribution to the thermodynamic heat capacity which increases with poorer crystallization (see Figures 10−13). This small amount of reversible latent heat was discovered only recently[13] but seems to exist for many semicrystalline polymers.[32,33] It can be seen from Figure 10 that the initial reversing heat capacity, as may be observed by TMDSC with an underlying heating rate, is much higher than the true reversible heat capacity approached at later times, since each subsequent modulation occurs at a higher temperature if there is an underlying heating rate. In the present case, the decrease in reversing, apparent heat capacity occurs with a relaxation time of 100 min at 299 K.

All of these observations must be combined to reach a more detailed description of the polymer morphology which ultimately may help to understand the changes in physical properties that occur without changes in crystallinity. The interplay of the various thermodynamic contributions is discussed first, and a possible morphology that may lead to the reversible latent heat contributions is summarized thereafter.

4.2. Contributions to the Apparent Heat Capacity. There are six different thermodynamic contributions to the apparent heat capacity in the melting and crystallization region of the analyzed polymer, as was concluded earlier.[13] The first three can be truly reversible, and the second three are increasingly irreversible. (1) The first and largest contribution to the thermodynamic heat capacity of polymers is always vibrational. The vibrational heat capacity has been calculated from the density of states of the skeletal and group vibrations,[45] as determined from normal mode calculations and matches to low-temperature, experimental heat capacities which were critically evaluated from more than 100 measurements in many different laboratories.[64] The skeletal vibrations contribute most of the low-temperature heat capacity and level at their limit of $2R$ at about 300 K ($c_v = 1.19$ J K^{-1} g^{-1}). The group vibrations start contributing at about 150 K, reach $1.4R$ by about 400 K ($c_v = 0.86$ J K^{-1} g^{-1}), and have a limit of $7R$ which would be approached only far above the decomposition temperature of the polymer.

(2) The second contribution originates from the emergence of dynamically changing conformational isomers. In polyethylene, the low-energy trans conformation can reach a local equilibrium with its two, higher-energy gauche conformations. For the glassy polymer this process starts somewhat above 100 K and for the crystalline polymer, above 250 K. At the beginning of the glass transition (237 K), this process contributes about 0.24 J K^{-1} g^{-1} to the heat capacity of the glass; at the equilibrium melting temperature (414.6 K), it contributes about 0.36 J K^{-1} g^{-1} to the specific heat capacity of the orthorhombic crystal.[65] For the amorphous polyethylene, the local trans−gauche processes change at the glass transition from a local to a global equilibrium, involving a cooperative process that extends over a small volume of perhaps 1 nm in diameter. In the glass-transition range, this cooperative process is slower than the calorimetry and may be not fully reversible until the temperature is sufficiently high so that the cooperative kinetics is faster than the rate of measurement. This reversibility is reached at the end of the glass transition, commonly identified as T_e.[27] The analysis by TMDSC allows the study of this cooperative kinetics of the glass transition.[66] The trans−gauche exchange is an internal rotation (conformational motion) between states of different potential energy. Calorimetrically, the change in conformation is most easily correlated to the change in potential energy. A change from torsional oscillation to internal rotation between conformational isomers of equal potential energy would change the heat capacity only negligibly. At both the disordering transition from the orthorhombic to the pseudohexagonal phase and to the melt, this increase in potential energy is a significant part of the latent heat of transition. The change in the trans-to-gauche ratio also causes much of the difference between the solid and liquid heat capacities of polyethylene.[67] At 250 K, the liquid specific heat capacity is 0.73 J K^{-1} g^{-1} higher than that of the orthorhombic crystals; at about 400 K, however, both heat capacities are about equal.[64]

(3) The third contribution is the reversible melting fraction to be discussed below. It has been observed some time ago that not all melting in polymers removes entire molecules from the crystals.[68] Rather, molecules may melt partially and can then not be extracted from the remaining semicrystalline, higher-melting fraction but can recrystallize at lower temperature or, as shown here, crystallize and melt reversibly. Not only must there be a crystal to obviate primary and secondary nucleation for a reversible crystallization and melting, but there must also be a molecular nucleus to initiate the reversible process.[25] It is of interest to note that linear paraffins up to at least $C_{50}H_{102}$ melt close to reversibly, in contrast to polymers and also to most other small molecules. Paraffins seem to need little or no crystal as well as molecular nucleation, while polymers need both, and most other small molecules need at least crystal nucleation.[24]

(4) Contribution four involves crystal perfection. Typically the perfected crystals melt 5−20 K above the annealing temperature, as demonstrated by the common annealing peaks.[25] For the copolymer of this research, details were reported recently[13] and can be seen in Figures 5 and 6. For the peak caused by annealing at 299 K, the relaxation time was about 100 min and the subsequent melting peak was at 312 K. The irreversibility of this process is indicated by the 13 K temperature difference. Early observation on the reduced ability of copolymers to reach extended-chain macroconformations[25,58,69] and more recent observation on the strongly reduced sliding diffusion in branched polyethylenes[70] led to the conclusion that the copolymers of this research are less likely to reorganize because in this process the branches would have to be drawn through the crystals. Melting, recrystallization, and additional remelting are most likely the only processes that occurs during heating or annealing at higher temperatures, besides full strand melting of unstable crystals. Reorganization already occurs during storage at room temperature for copolymers having a comonomer content higher than 2.1 mol % of 1-octene.[70]

(5, 6) Contribution five is usually identified as secondary crystallization; i.e., it involves less perfect crystal growth which occurs later than observed for the initial crystals. Contribution six is the well-studied initial crystallization.[25] The analysis of the thermodynamic stability of both primary and secondary crystals is complicated by crystal perfection, even when growth occurs isothermally. The interpretation of the irreversibility of the secondary crystallization is obscured by the existence of a global network of the primary crystals. Typical data for primary and secondary crystallization of linear polyethylene nucleated at 398.7 and 401.2 K with extended-chain crystals from the melt were presented some time ago.[25,71] A time constant of approximately 5 min was found for the secondary crystallization of the present polymer at 299 K.[13] Contribution 5 may also contribute to the annealing peak. For homopolymers, contribution 6, the primary crystallization, yields commonly the biggest latent heat effect. Overall, the ordering of polymers may go to fully ordered crystals, but mesophases are also possible, such as liquid crystals and condis crystals.[55] Crystals, condis, and smectic liquid crystals are often only of nanophase or

microphase dimensions, while nematic liquid crystals are usually of macroscopic domain size.[72]

This research on poly(ethylene-*co*-1-octene) clearly shows all six caloric effects just summarized. A series of homopolymers analyzed recently with TMDSC show that this nonreversing and reversing behavior of melting, crystallization, and annealing seem to occur universally in flexible macromolecules. The homopolymers analyzed in our laboratory were poly(oxyethylene),[33] poly(ethylene terephthalate),[32] poly(trimethylene terephthalate),[73] and polydioxanone.[74] We expect, thus, that the described processes in this paper have rather broad applicability to the field of polymers, and their understanding will permit a better link between structure and properties.

4.3. Reversible Melting. The initial reversing apparent heat capacity decreases considerably with time, attesting to the dynamic overall crystal morphology (see Figure 10). Only after times beyond about 100 min at 299 K has one reached the final, metastable, global structure within which only the fully reversible process remains. The level of the reversible, apparent heat capacity decreases exponentially with a decreasing cooling rate by about 0.02 J K^{-1} g^{-1} (decade of cooling rate)$^{-1}$, as shown in Figure 12. This decrease could be caused by either or both of the following contributions: (a) a reduced heat capacity and (b) a reduced latent heat contribution from a reversible crystallization and melting. Of the three reversible contributions discussed in section 4.2, the vibrational contribution (1) does not change significantly when changing the structure or morphology of a sample and can be omitted from the discussion. Even the liquid has a similar vibrational contribution as the solid.[67]

Contribution 2 would go in the right direction at the temperature of interest, 299 K. The poorer crystallized pseudohexagonal phase has a higher heat capacity due to a larger gauche concentration.[75] One would, however, not expect a specific heat capacity higher than that of the liquid polyethylene of 2.20 J K^{-1} g^{-1}.[64] The apparent specific heat capacities of the quenched and the sample cooled at 10 K min^{-1} are, in contrast, 2.50 and 2.44 J K^{-1} g^{-1} (see Figure 12). However, even the quenched sample is far from amorphous, as can easily be seen from the standard DSC heating scan shown in Figure 6. On the basis of these considerations one can identify contribution 3, a latent heat, as the major cause of the increased reversible heat capacity. Over a 20 K temperature range the two samples would need to change 2.0 and 1.6% in reversible crystallinity, respectively, when calculating with the orthorhombic heat of fusion or about double as much when using the estimate for the pseudohexagonal heat of fusion. Contributions 4−6 can be excluded because of their supercooling of ≥13 K, which exceeds the temperature-modulation amplitude by a factor of more than 6 as can be seen from Figures 1 and 2.

A remaining point of discussion is to propose the scenario for the stepwise growth of crystal morphology. Naturally, this involves a reasonable amount of speculation and points toward further experimentation, needed to prove the details and give more quantitative information. Atomic force microscopy and microcalorimetry[76] may be new tools that can pinpoint some of the morphological and structural features.[77]

On very slow cooling, or with help of self-nucleation, the poly(ethylene-*co*-1-octene) sets up a network of mainly orthorhombic crystal lamellae, using the randomly occurring long sequences of ethylene in the copolymer. This early stage of crystallization may be described by the kinetics developed by Baur, making use of Flory's theory of crystallization of copolymers.[78] These crystals are linked rather quickly by amorphous defects[58,75] and set up a metastable, global network of interlinked crystals. From Figure 3 one would guess that this type of gelation is reached at 5% of crystallization.

On faster cooling and by removal of self-nucleation, increasingly the longer sequences do not crystallize fast enough into orthorhombic crystals and contribute to the metastable mesophase. Its crystallization does not have to undergo as much diffusional segregation and molecular nucleation. Ultimately, it sets up the same type of global crystal network, although the actual number of segments that are involved in this initial, quick crystallization may be bigger (crystallization peaks in Figures 1a and 2). Certainly, with faster cooling, the global network involves more of the shorter ethylene sequences, and longer sequences are more often included in smaller crystals. The poorer the initial crystals, the less is the distance between crystallization and zero entropy production melting temperature (the temperature of melting without change in metastability), and the larger is the trend to annealing.[26] The annealing behavior of the present sample was detailed before for different molecular structures,[13] and the larger amounts of reversing and reversible melting are supported by this scenario.

After the crystal network is set up, the amorphous defects can continue locally to crystallize with very little or no long-distance diffusion in a secondary crystallization process. It was shown before that this process can be described with a relaxation time of about 5 min at 299 K.[13] This crystallization is related to cold crystallization, a crystallization that is well-known for crystallization of glassy polymers close to the glass transition temperature.[79] In the present example, this secondary crystallization makes up more than $^3/_4$ of the total crystallization (see Figure 3). This crystallization can involve an addition of chain segments to existing crystal or mesophase surfaces, or at sufficiently low temperature, it may also involve separate crystallization of CH_2− sequences that are sufficiently long to have reached their equilibrium melting temperature. It is well-known that a side chain of sufficient length to be decoupled from the polymer backbone will crystallize at similar temperatures as the corresponding small molecules.[26] One can assume that backbone chains segments can similarly be decoupled between crystals. For a crystallization between 310 and 250 K, this would correspond to crystallization of sequences of from 20 to 10 CH_2− groups, respectively. The fraction of crystallizable units of 10 or more methylene units in the analyzed copolymer can be calculated from the molar branch concentration as 0.47 [$= (1.00 - 0.073)^{10}$], which is the proper order of magnitude for the observed maximum mesophase crystallinity.

The increased reversible heat-flow rate is, thus, due to the latent heat effect (3) which may be caused either by isolated crystals, which crystallize and melt in a local equilibrium set up within the network of primary and secondary crystals (5, 6) after their rearrangement has ceased (4), or by reversible crystallization and melting on the lateral surface areas of the crystals (5, 6). In the

first case the reversibly growing crystals are attached to the chains leaving the (001) or related surfaces, while the second case is linked to the lateral growth faces changing the size of crystals (5, 6). Crystals grown as (5, 6) could not increase in the chain direction because this would lead to more stable crystals which would not support a low-temperature, local equilibrium, but rather be an annealing which is not reversible.

Well-crystallized, high-density orthorhombic polyethylene with less than 3 CH_3 per 1000 carbon at the backbone of perhaps more than 80% total crystallinity exhibits a degree of reversibility of about 0.07% per kelvin.[41] The poly(ethylene-*co*-1-octene) used in this study has a total mesophase crystallinity of close to 20% at ambient temperature (double the equivalent of the orthorhombic crystallinity of Figure 3), and its degree of reversibility is about 0.1% per kelvin. If the mechanism of the structural change would be the same in both cases, we needed to observe an about 4 times larger number of surface chain segments, which is easily accounted for either by larger numbers of such surface chains or by crystals with 50% smaller lateral extensions. It seems that the degree of reversibility of crystallization and melting is closely related to the crystal morphology. Therefore, the degree of reversibility of crystallization and melting may be used to judge the crystal morphology, i.e., the volume-to-surface-ratio, and perhaps the ratio between lateral surface area and basal plane surface area and the degree of perfection of the crystal surfaces. We believe that the latter ideas are universal and not only applicable to the particular class of copolymers investigated in this study.

Acknowledgment. The authors thank J. S. Lin (Oak Ridge National Laboratory) for assistance in SAXS experiments, A. Wutzler (Martin-Luther-University Halle-Wittenberg, Germany) for performing and discussion of FTIR measurements, and the group of V.B.F. Mathot (Catholic University Leuven, Belgium) for general discussions. This work was supported by the Division of Materials Research, National Science Foundation, Polymers Program, Grant DMR-9703692, and the Division of Materials Sciences and Engineering, Office of Basic Energy Sciences, U.S. Department of Energy at Oak Ridge National Laboratory, managed and operated by UT-Batelle, LLC, for the U.S. Department of Energy, under Contract DOE-AC05-00OR22725.

References and Notes

(1) Bensason, S.; Minick, J.; Moet, A.; Chum, S.; Hiltner, A.; Baer, E. *J. Polym. Sci., Polym. Phys.* **1996**, *34*, 1301.
(2) McFaddin, D. C.; Russell, K. E.; Wu, G.; Heyding, R. D. *J. Polym. Sci., Polym. Phys.* **1993**, *31*, 175.
(3) Androsch, R.; Blackwell, J.; Chvalun, S. N.; Wunderlich, B. *Macromolecules* **1999**, *32*, 3735.
(4) Androsch, R.; Wunderlich, B.; Blackwell, J.; Chvalun, S. N. Presented at the APS Centennial Meeting March 20−26, Atlanta, GA; *Bull. Am. Phys. Soc.* **1999**, *44* (2), 1562.
(5) Keating, M. Y.; Lee, I. *J. Macromol. Sci., Phys.* **1999**, *B38*, 379.
(6) Schulze, U.; Arndt, M.; Freidanck, F.; Beulich, I.; Pompe, G.; Meyer, E.; Jehnichen, D.; Pionteck, J.; Kaminsky, W. *J. Macromol. Sci., Pure Appl. Chem.* **1998**, *A35*, 1037.
(7) Alizadeh, A.; Richardson, L.; Xu, J.; McCartney, S.; Marand, H.; Cheung, Y. W.; Chum, S. *Macromolecules* **1999**, *32*, 6221.
(8) Mathot, V. B. F.; Scherrenberg, R. L.; Pijpers, T. F. J.; Engelen, Y. M. T. Structure, crystallization and morphology of homogeneous ethylene−propylene, ethylene−1-butene, and ethylene−1-octene copolymers with high comonomer contents. In *New Trends in Polyolefin Science and Technology*; Hosoda, S., Ed.; Research Signpost: Trivandrum, India, 1996; p 71.
(9) Mathot, V. B. F.; Scherrenberg, R. L.; Pijpers, T. F. J. *Polymer* **1998**, *39*, 4541.
(10) Mathot, V. B. F.; Scherrenberg, R. L.; Pijpers, T. F. J.; Bras, W. *J. Therm. Anal.* **1998**, *46*, 681.
(11) Mathot, V. B. F.; Pijpers, M. F. J. *J. Appl. Polym. Sci.* **1990**, *39*, 979.
(12) Androsch, R. *Polymer* **1999**, *40*, 2805.
(13) Androsch, R.; Wunderlich, B. *Macromolecules* **1999**, *32*, 7238.
(14) Wunderlich, B. *J. Polym. Sci., Part C* **1963**, *1*, 41.
(15) Reading, M.; Hahn, B. K.; Crowe, B. S. U.S. Patent, Method and Apparatus for Modulated Differential Analysis, July 6, 1993; 5,224,775.
(16) Gill, P. S.; Sauerbrunn, S. R.; Reading, M. *J. Therm. Anal.* **1993**, *40*, 931.
(17) Reading, M.; Elliot, D.; Hill, V. L. *J. Therm. Anal.* **1993**, *40*, 949.
(18) Wunderlich, B.; Jin, Y.; Boller, A. *Thermochim. Acta* **1994**, *238*, 277.
(19) Wunderlich, B. *J. Therm. Anal.* **1997**, *48*, 207.
(20) Toda, A.; Oda, T.; Hikosaka, M.; Saruyama, Y. *Thermochim. Acta* **1997,** *293*, 47. Toda, A.; Tomita, C.; Hikosaka, M.; Saruyama, Y. *Polymer* **1998**, *39*, 5093.
(21) Schawe, J. E. K.; Winter, W. *Thermochim. Acta* **1999**, *330*, 85. Schawe, J. E. K.; Bergmann, E.; Winter, W. *J. Therm. Anal.* **1998**, *54*, 565. Schawe, J. E. K.; Bergmann, E. *Thermochim. Acta* **1997,** *304/305*, 179.
(22) Chen, W.; Toda, A.; Wunderlich, B. *Proc. 26th NATAS Conf., Cleveland, OH, Sept 13−15, 1998* **1998**, *26*, 157. Chen, W.; Toda, A.; Moon, I.; Wunderlich, B. *J. Polym. Sci., Polym. Phys.* **1999**, *37*, 1539.
(23) Wunderlich, B.; Boller, A.; Okazaki, I.; Ishikiriyama, K.; Chen, W.; Pyda, M.; Pak, J.; Moon, I.; Androsch, R. *Thermochim. Acta* **1999**, *330*, 21.
(24) Pak, J.; Boller, A.; Moon, I.; Pyda, M.; Wunderlich, B. *Thermochim. Acta* **2000**, *357/358*, 259. Androsch, R.; Wunderlich, B. *Thermochim. Acta* **2000**, paper 1, in print; paper 2, submitted.
(25) Wunderlich, B. *Macromolecular Physics*; Academic Press: New York, 1976; Vol. 2.
(26) Wunderlich, B. *Macromolecular Physics*; Academic Press: New York, 1980; Vol. 3.
(27) Wunderlich, B. *Thermal Analysis*; Academic Press: New York, 1990. For an update and expansion see: *Thermal Analysis of Materials*, a computer-assisted course of 36 lectures and 2879 screen pages, published on the Internet (web.utk.edu/~athas/courses/tham99.html), downloadable including presentation software, University of Tennessee, Knoxville, TN, 2000.
(28) Binsbergen, F. L. Thesis, Groningen 1969; *Polymer* **1970**, *11*, 253. Binsbergen, F. L.; DeLange, B. G. M. *Polymer* **1970**, *11*, 309. Binsbergen, F. L. *J. Polym. Sci., Polym. Phys.* **1973**, *11*, 117.
(29) Wunderlich, B.; Mehta, A. *J. Polym. Sci., Polym. Phys.* **1974**, *12*, 255; *Colloid Polym. Sci.* **1975**, *253*, 193.
(30) Kovacs, A. J.; Gonthier, A.; Straupe, C. *J. Polym. Sci., Polym. Symp.* **1977**, *50*, 283. Kovacs, A. J.; Straupe, C.; Gonthier, A. *J. Polym. Sci., Polym. Symp.* **1980**, *59*, 31.
(31) Cheng, S. Z. D.; Wunderlich, B. *J. Polym. Sci., Polym. Phys.* **1986**, *24*, 595.
(32) Okazaki, I.; Wunderlich, B. *Macromolecules* **1997**, *30*, 1758; *Macromol. Chem. Phys., Rapid Commun.* **1997**, *18*, 313.
(33) Ishikiriyama, K.; Wunderlich, B. *Macromolecules* **1997**, *30*, 4126; *J. Polym. Sci., Polym. Phys.* **1997**, *35*, 1877.
(34) Schick, C.; Merzlyakov, M.; Wunderlich, B. *Polym. Bull.* **1998**, *40*, 297.
(35) Wurm, A.; Merzlyakow, M.; Schick, C. *J. Therm. Anal.* **1999**, *56*, 1155.
(36) Wurm, A.; Merzlyakow, M.; Schick, C. *Colloid Polym. Sci.* **1998**, *276*, 289.
(37) Albrecht, T.; Strobl, G. *Macromolecules* **1995**, *28*, 5827.
(38) Tanabe, Y.; Strobl, G. R.; Fischer, E. W. *Polymer* **1986**, *27*, 1147.
(39) Strobl, G. R.; Schneider, M. J.; Voigt-Martin, G. *J. Polym. Sci., Polym. Phys.* **1980**, *18*, 1361.
(40) Schultz, J. M.; Fischer, E. W.; Schaumburg, O.; Zachmann, H. A. *J. Polym. Sci., Polym. Phys.* **1980**, *18*, 239.
(41) Hu, W.; Albrecht, Th.; Strobl, G. *Macromolecules* **1999**, *32*, 7548.
(42) Peeters, M.; Goderis, B.; Vonk, C.; Reynaers, H.; Mathot, V. *J. Polym. Sci., Polym. Phys.* **1997**, *35*, 2689.

(43) Wagner, J.; Abu-Iqyas, S.; Monar, K.; Phillips, P. J. *Polym. Commun.* **1999,** *40*, 4717. Kim, M.; Phillips, P. J. *J. Appl. Polym. Sci.* **1998**, *70*, 31.
(44) Magonov, S.; Androsch, R., unpublished data by atomic force microscopy (AFM), 1998. See also: Magonov, S.; Godovski, Y. *Am. Lab.* **1999**, *31*, 55.
(45) Wunderlich, B. Advanced *TH*ermal *A*nalysis *S*ystem; *Pure and Appl. Chem*. **1995**, *67*, 1919. For downloadable data use the Internet URL: web.utk.edu/∼athas.
(46) Gaur, U.; Wunderlich, B. *Macromolecules* **1980**, *13*, 445.
(47) Wunderlich, B.; Czornyj, G. *Macromolecules* **1977**, *10*, 906.
(48) Androsch, R.; Moon, I.; Kreitmeier, S.; Wunderlich, B. *Thermochim. Acta* **2000**, *357*, 267.
(49) Androsch, R.; Wunderlich, B. *Thermochim. Acta* **1999**, *333*, 27.
(50) Androsch, R. *J. Therm. Anal. Calorimetry* **2000**, *61*, 75.
(51) Blundell, D. J.; Keller, A.; Kovacs, A. J. *J. Polym. Sci., Polym. Lett.* **1966**, *4*, 481.
(52) Vidotto, P. G.; Levy, D.; Kovacs, A. J. *Kolloid Z. Z. Polym.* **1969**, *230*, 19.
(53) Vonk, C. G.; Pijpers, A. P. *J. Polym. Sci., Polym. Phys.* **1985**, *23*, 2517.
(54) Androsch, R., manuscript in preparation for submission to *Macromolecules* in 2000. The interplanar spacing d_{200} of the orthorhombic structure, which in the case of poly(ethylene-*co*-1-octene) can safely be determined in film patterns and is not overlapping with the 100 reflection of the pseudohexagonal phase like the 110 reflection of the orthorhombic phase, increases systematically with the comonomer content. A similar shift of d_{200} is observed for poly(ethylene-*co*-1-hexene); however, in the latter case the shift is more distinct.
(55) Wunderlich, B.; Möller, M.; Grebowicz, J.; Baur, H. *Conformational Motion and Disorder in Low and High Molecular Mass Crystals*; Springer-Verlag: Berlin, 1988 (*Adv. Polym. Sci.* Vol. 87).
(56) Kwon, Y. K.; Boller, A.; Pyda, M.; Wunderlich, B. *Polymer* **2000**, *41*, 6237.
(57) Crist, B.; Morosoff, N. *J. Polym. Sci., Polym. Phys.* **1973**, *11*, 1023. Matyi, R. J.; Crist, B. *J. Polym. Sci., Polym. Phys.* **1978**, *16*, 1329.
(58) Wunderlich, B. *Macromolecular Physics*; Academic Press: New York, 1973; Vol. 1.
(59) Stein, R. S. *J. Chem. Phys.* **1955**, *23*, 734. Keller, A.; Sandemann, I. *J. Polym. Sci.* **1955**, *15*, 133. Kaiser, R. *Kolloid Z. Z. Polym.* **1956**, *148*, 168; **1956** *149*, 84; **1957**, *152*, 8. Hendus, H.; Schnell; G. *Kunststoffe* **1961**, *51*, 69. Luongo, J. P. *J. Polym. Sci., Polym. Lett.* **1964**, *2*, 75.
(60) Talsky, G.; Mayring, L.; Kreuzer, H. *Angew. Chem.* **1978**, *90*, 840, 563.
(61) Holland-Moritz, K.; van Werden, K. *Makromol. Chem.* **1981**, *182*, 651.
(62) Seidel, H. H, Ph.D. Thesis, Köln, Germany,1988.
(63) Painter, P. C.; Havens, J.; Hart, W. W.; Koenig, J. L. *J. Polym. Sci., Polym. Phys.* **1977**, *15*, 1237.
(64) Gaur, U.; Wunderlich, B. *J. Phys. Chem. Ref. Data* **1981**, *10*, 119.
(65) Wunderlich, B. *J. Chem. Phys.* **1962**, *37*, 2429; *Thermochim. Acta* **1997**, *300*, 43.
(66) Wunderlich, B.; Boller, A.; Okazaki, I.; Kreitmeier, S. *J. Therm. Anal.* **1996**, *47*, 1013.
(67) Pyda, M.; Wunderlich, B. *Macromolecules* **1999**, *32*, 2044.
(68) Mehta, A.; Wunderlich, B. *Makromol. Chem.* **1974**, *175*, 977.
(69) Arakawa, T.; Wunderlich, B. *J. Polym. Sci., Part A-2* **1966**, *4*, 53.
(70) Peeters, M.; Goderis, B.; Reynaers, H.; Mathot, V. *J. Polym. Sci., Part B: Polym. Phys. Ed.* **1999**, *37*, 83.
(71) Wunderlich, B.; Melillo, L.; Cormier, C. M.; Davidson, T.; Snyder, G. *J. Macromol. Sci.* **1967**, *B1*, 485.
(72) Chen, W.; Wunderlich, B. *Macromol. Chem. Phys.* **1999**, *200*, 283.
(73) Pyda, M.; Boller, A.; Grebowicz, J.; Chuah, H.; Lebedev, B. V.; Wunderlich, B. *J. Polym. Sci., Part B: Polym. Phys.* **1998**, *36*, 2499. Pyda, M.; Wunderlich, B. *J. Polym. Sci., Part B: Polym. Phys.* **2000**, *38*, 622. See also: *Proc. 27th NATAS Conf. Savannah, GA, Sept 19*−*22* **1999**, *27***,** 21.
(74) Ishikiriyama, K.; Pyda, M.; Zhang, G.; Forschner, T.; Grebowicz, J.; Wunderlich, B. *J. Macromol. Sci., Phys.* **1998**, *B37*, 27.
(75) Wunderlich, B.; Sumpter, B. G.; Noid, D. W.; Liang, G. L. Computer Simulation of Macromolecular Crystals and Their Defects. In *Ordering in Macromolecular Systems*; Teramoto, A., Kobayashi, M., Norisuje, T., Eds.; Springer-Verlag: Berlin, 1994; pp 35−49.
(76) Moon, I.; Androsch, R.; Chen, W.; Wunderlich, B. *J. Therm. Anal. Calorimetry* **2000**, *59*, 187.
(77) Wunderlich, B. Temperature-Modulated Calorimetry in the 21st Century. *Thermochim. Acta* **2000**, *355*, 43.
(78) Baur, H. *Kolloid Z. Z. Polym.* **1965**, *203*, 97; **1968**, *224*, 36; *Ber. Bunsen-Ges.* **1967**, *71*, 703.
(79) Wunderlich, B. *J. Chem. Phys.* **1958**, *29*, 1395.

MA000504H